The Faraday effect in semimagnetic semiconductors

P. I. Nikitin and A. I. Savchuk

Institute of General Physics, Academy of Sciences of the USSR, Moscow; State University, Chernovtsy
Usp. Fiz. Nauk **160**, 167–196 (November 1990)

A review of experimental and theoretical research on the Faraday effect in a new class of materials–semimagnetic semiconductors (SMS). The authors discuss the mechanism responsible for the giant Faraday effect in SMS, which is based on s, p–d exchange interactions of excitons, electrons, and holes with magnetic ions. The authors also examine the dependence of Faraday rotation (FR) on wavelength, magnetic component concentration, temperature, and magnetic field intensity in $A^2B^6\langle Mn\rangle$ and $A^2_{1-x}Mn_xB^6$ crystals, as well as other SMS ($GaAs\langle Mn\rangle$, $CdP_2\langle Mn\rangle$, $Pb_{1-x}Mn_xI_2$). They examine the use of FR in the study of the paramagnetic–spin glass transition, the role played by relaxation processes involving magnetic Mn^{2+} ions, excitons, and polarons in the direct and inverse Faraday effects, and the properties of FR in thin SMS films and spin superlattices. Finally, the authors analyze possible applications of the Faraday effect in SMS to practical magnetooptic devices (optical isolators, fiber optic magnetic field sensors).

1. INTRODUCTION

Semimagnetic semiconductors (SMS) comprise a new class of materials that combine the properties of ordinary and magnetic semiconductors (other designations used in the literature include dilute magnetic semiconductors, and magnetically mixed or magnetically doped semiconductors). These materials include semiconductor crystals doped with 3d-ions of transition metals and solid solutions containing a magnetic component. The intense research effort into SMS originated in the early studies of manganese-doped crystals[1] and $Cd_{1-x}Mn_xTe$ solid solutions,[2] which reported giant spin splittings in the band states of electrons, holes, and excitons, as well as a giant Faraday effect caused by the exchange interaction between band carriers and localized magnetic moments of Mn^{2+} ions. The striking aspect of these effects was that a relatively small external magnetic field (of $H \approx 30$ kOe intensity) induced a large spin splitting of the exciton line (up to tens of meV) and significantly enhanced the Faraday rotation (FR) in the appropriate spectral range.

The fundamental qualitative difference between SMS and ordinary semiconductors (for example, between $Cd_{1-x}Mn_xTe$ and $Cd_{1-x}Zn_xTe$) is that in SMS an external magnetic field induces a significant exchange interaction between magnetic ions and charge carriers in the bands. In the absence of an external field, however, electronic processes and modifications of the band structure as a function of x are quite similar in these two classes of crystals.

On the other hand, SMS also can be viewed as an intermediate class of materials lying between magnetic and nonmagnetic semiconductors. By varying the magnetic component concentration together with the external parameters (temperature, magnetic field), one can induce a transition from one type of semiconductor to the other and extract the properties introduced by the appearance of localized magnetic moments.

In this review we will restrict ourselves to a summary of the available information on one of the several novel effects in SMS–the Faraday effect. We believe that this effect most fully reflects the specific properties of these new materials, combining two fundamental branches of physics–optics and magnetism. Notably, in addition to its scientific importance, the Faraday effect in SMS holds promise for real technological applications.

We should note that several review articles devoted to SMS have already been published.[3–9] These reviews do not devote sufficient attention to the Faraday effect, however, and hence do not give a full picture of this direction in SMS research.

Among the several topics discussed in this review, we will begin with an analysis of the magnetooptic activity enhancement in SMS (Section 2), since an understanding of the mechanisms responsible for the giant FR effect is crucial to both the physics and the possible practical applications of SMS. Our analysis will proceed from the standard semiconductor description, where the rotation of the optical polarization plane is largely determined by the Zeeman splitting of the energy levels in an external magnetic field. In wide-gap SMS, such as $Cd_{1-x}Mn_xTe$ crystals, the relevant types of electronic processes include exciton, interband, and intraband transitions; intracenter transitions in the Mn^{2+} ions; and transitions involving impurities and lattice defects. At low temperatures the region near the fundamental absorption edge is dominated by exciton transitions, and hence the giant spin splitting of the main exciton peak caused by the external magnetic field is the key to FR enhancement in SMS. The magnitude of the Faraday effect in SMS is directly related to the exchange interaction constants between magnetic ions and band carriers that make up the exciton pairs, and is proportional to the magnetization of the magnetic subsystem. Nonetheless, the exciton contribution can vary strongly as a function of optical wavelength, magnetic ion concentration, and temperature, so that in some cases contributions from other types of transitions to the total effect can be important.

An analysis of experimental results for a number of SMS systems presented in Sections 3, 4 supports the validity of the above approach, while the observed anomalies in the spectral, concentration, and temperature dependences of FR confirm the existence of at least three contributing processes.

Depending on temperature and magnetic component concentration, semimagnetic semiconductors can form diamagnetic, paramagnetic, antiferromagnetic, and ferromag-

 0038-5670/90/110974-16$01.00

netic states, as well as a spin glass state. The Faraday effect has proved to be quite effective in the study of the paramagnetic–spin glass transition (Section 5). Recall that a spin glass is actually a disordered magnetic material in which the magnetic moments are "frozen" in a chaotic fashion below some critical temperature T_s.[10] A characteristic property of spin glasses is that cooling a sample in a magnetic field and switching on the field after cooling below T_s tend to produce different values of the magnetic moment. This difference can be monitored by measuring FR in SMS samples with different cooling histories. Faraday rotation data make it possible to establish the phase transition temperature T_s and hence construct the magnetic phase diagram of the SMS system. The use of the Faraday effect in the study of the paramagnetic–spin glass transition is also important because it can elucidate the mechanisms responsible for spin glass formation in systems other than SMS.

There have been predictions that exchange interactions between electrons and magnetic ions in SMS should lead to large light-induced spin polarization. Indeed, magnetization by intense, circularly polarized radiation, also known as the inverse Faraday effect, has been observed in $Cd_{1-x}Mn_xTe$ and $Hg_{1-x}Mn_xTe$ SMS materials (Section 8). Contrary to predictions, however, the magnitude of this effect turned out to be very small. In the particular case of $Hg_{1-x}Mn_xTe$ crystals, the anomalously small value of the inverse Faraday effect can be attributed to magnetic moment transfer from the magnetic ion subsystem to the hole subsystem, i.e., the formation of an effective leakage channel for the optically induced magnetization of the magnetic subsystem. Still, the observation of the inverse Faraday effect in SMS is of fundamental importance, since it can yield new information on spin exchange and spin-lattice relaxation processes in such crystals.

The earlier investigations of SMS materials were carried out on bulk samples, usually grown by the Bridgman technique. In recent years thin SMS films (Section 9) have attracted much attention due to advances in the epitaxial fabrication of thin semiconductor layers. Multilayered structures known as spin superlattices[11] proved particularly interesting. As it turned out, many of the magnetooptic effects discovered in bulk SMS crystals carry over to thin films. Furthermore, by varying the layer thickness in spin superlattices one can observe new phenomena in FR due to quantum confinement of electrons in the wells (layers).

The growing interest in bulk SMS crystals, as well as thin film and multilayered structures, is undoubtedly due to the possible practical applications of SMS materials. Although the arsenal of techniques that can be employed in SMS research is still far from exhausted, these materials have already been employed in various magnetooptic devices. In Section 10 we will describe the applications of SMS in nonreciprocal systems (optical isolators) and high-frequency fiber optic magnetic field sensors—devices based on the giant Faraday effect in these materials.

2. THEORETICAL DESCRIPTION OF THE FARADAY EFFECT ENHANCEMENT IN SEMIMAGNETIC SEMICONDUCTORS (SMS)

The Faraday effect, discovered by Michael Faraday in 1845, consists of the rotation of the plane of polarization of linearly polarized light propagating through a medium placed in a longitudinal magnetic field H.[12] Phenomenologically, the Faraday effect is due to the magnetically induced difference in the properties of the medium for right- and left-polarized components of the radiation. The angle θ by which the plane of polarization rotates can be expressed as follows:[13]

$$\theta = \frac{Ed}{2\hbar c}(n^-(E) - n^+(E)), \tag{2.1}$$

where $E = \hbar\omega$ is the photon energy; ω is the frequency; d is the distance traversed in the medium; c is the speed of light in vacuum; $n^\pm$ is the index of refraction (where the + and − subscripts label the two opposite circular polarizations $\sigma^\pm$).

In a quantum mechanical description, the difference $\Delta n^\pm(E)$ arises from the effect of the magnetic field on electronic transitions between levels i and j with energies $E_{i,j}$:

$$n^-(E) - n^+(E) = \frac{\partial n}{\partial E}\Delta E_{ij}. \tag{2.2}$$

Then

$$\theta = \frac{Ed}{2\hbar c}\frac{\partial n}{\partial E}\Delta E_{ij}, \tag{2.3}$$

where ΔE_{ij} is the energy difference between transitions observed in σ^+ and σ^- polarizations.

The interaction of electromagnetic radiation of wavelength λ with a semiconductor crystal induces various types of electronic transitions (exciton, interband, intraband, etc.). All these contribute to the Faraday effect to some extent.

If we restrict our attention to the region near the fundamental absorption edge, exciton transitions are the dominant process. Then one can turn to the single Lorentz oscillator model[14] and express the refraction index as

$$n^2 = n_0^2 + F_0(E_0^2 - E^2)^{-1}; \tag{2.4}$$

where E_0 is exciton transition energy; F_0 is a constant that incorporates the oscillator strength f_0 of the exciton transition; n_0 contains of all other contributions.

Neglecting n_0 at photon energies close to E_0, the above formula can be used to obtain[14]

$$\theta = \frac{F_0^{1/2}d}{2\hbar c}\frac{E^2}{(E_0^2 - E^2)^{3/2}}\Delta E_0. \tag{2.5}$$

The foregoing provides the basic framework for studying the Faraday effect in most wide-gap semiconductors. In the particular case of SMS materials one should introduce strong s-, p–d exchange interactions, which produce large spin splittings ΔE_0 of band and exciton states.

The exchange interaction between band carriers and localized $3d$-electrons of Mn^{2+} ions can be described by a Heisenberg-type Hamiltonian

$$\mathscr{H}_{ex} = -\sum_{R_i} J(\mathbf{r} - \mathbf{R}_i)\, S_i s, \tag{2.6}$$

where $J(\mathbf{r}-\mathbf{R}_i)$ is the exchange integral between the band carriers and the magnetic moment of the Mn ion; $\hat{s}$ and $\hat{S}_i$ are the spin operators of band and localized electrons, respectively.

An example of the spin splitting of valence and conduction bands in $A^{II}{}_{1-x}Mn_xB^{VI}$ crystals caused by the exchange interaction (the diagonal part of (2.6)) is shown schematically in Fig. 1. Only optically allowed transitions for σ^+ and σ^- polarizations are shown, since these are

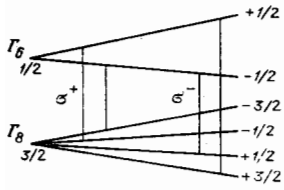

FIG. 1. Illustration of the Faraday effect in SMS: optical transition diagram between Γ_6 and Γ_8 states of $Cd_{1-x}Mn_xTe$ split by an external magnetic field.

responsible for the Faraday effect.

The magnitude of the spin splitting of the exciton term ΔE_0 is obtained by adding the spin splittings of the appropriate bands

$$\Delta E_0 = E_{\sigma^-}\left(\frac{3}{2}, \frac{1}{2}\right) - E_{\sigma^+}\left(-\frac{3}{2}, -\frac{1}{2}\right) = \frac{J_h - J_e}{g_{Mn}\mu_B} M, \tag{2.7}$$

$$M = -g_{Mn}\mu_B x N_0 \langle S_z \rangle, \tag{2.8}$$

while the FR angle θ is ultimately given by the following expression:[14]

$$\theta = \frac{F_0^{1/2} d}{2\hbar c} \frac{E^2}{(E_0^2 - E^2)^{3/2}} N_0 x (J_h - J_e) \langle S_z \rangle, \tag{2.9}$$

where M is the magnetization per unit volume; $\langle S_z \rangle$ is the thermodynamically averaged projection of Mn^{2+} ion spins along the magnetic field H; $g_{Mn} = 2$ is the spectroscopic splitting factor of Mn d-electrons; μ_B is the Bohr magneton; $J_{e,h}$ are the exchange interaction integrals of Mn^{2+} ions with electrons and holes.

In analyzing the effect in $Cd_{1-x}Mn_xTe$ crystals, Awschalom and co-workers[15] expressed F_0 in terms of the oscillator strength f_0 and plasma energy E_p, obtaining

$$\theta = \frac{19}{18} \frac{\pi}{n\lambda} \frac{E_p^2 E_0}{(E_0^2 - E^2)^2} f_0 J_h N_0 x \langle S_z \rangle. \tag{2.10}$$

They also took into account that $J_e/J_h = -0.25$ in $Cd_{1-x}Mn_xTe$. One can easily verify that the functional dependence $\theta(E)$ agrees with (2.9) by substituting $n = E_p f_0/(E_0^2 - E^2)^{1/2}$ into (2.10).

It follows from the analytic expressions (2.9), (2.10) for the Faraday effect in SMS that their principal difference from ordinary semiconductors[13] consists of the factors $J_{e,h}$ and $\langle S_z \rangle$ that enter into $\theta(E)$ and characterize the exchange interaction of electrons, holes, and excitons with localized spin moments of magnetic ions. Together with the exciton oscillator strength f_0 these parameters in fact determine the magnitude of the giant FR in SMS.

The enhancement of the Faraday effect in SMS can also be treated within the framework of the effective exchange field[16] which causes a large quasi-Zeeman splitting of the energy levels and produces an additional FR term that can markedly exceed the Faraday effect observed in ordinary, nonmagnetic semiconductors.

Experimental studies of FR in various SMS (which will be described separately in Sections 3, 4) indicate that the exciton contribution to $\theta(E)$ should be complemented with the contributions of other electronic transitions. Thus, the authors of Refs. 17–19 proposed the existence of three contributions with opposite signs in the Faraday effect in $Cd_{1-x}Mn_xTe$: interband term $\theta_1(E) \sim A_1(E_g - E)^{-1/2}$; exciton term $\theta_2(E) \sim A_2(E_0 - E)^{-2}$; and intracenter term $\theta_3(E) \sim A_3 E^2/(E_{eff}^2 - E^2)$. In Ref. 20 the experimental curves for the $Pb_{1-x}Mn_xI_2$ SMS were also approximated by a sum of the interband and exciton terms

$$\theta(E) = \theta_1(E) + \theta_2(E), \tag{2.11}$$

where, moreover, the spectral dependence of the corresponding FR contributions was described by the following formulae

$$\theta_1(E) = A_1 \frac{E_g^{3/2}}{E} [(E_g - E)^{-1/2} - (E_g + E)^{-1/2} - E E_g^{-3/2}], \tag{2.12}$$

$$\theta_2(E) = A_2 \frac{E_0 E}{(E_0 - E)^2} \left(1 + \frac{\hbar\Delta_{LT}}{E_0 - E}\right)^{1/2} \times \left[1 - \frac{\Gamma^2}{4(E_0 - E)^2}\left(1 + \frac{\hbar\Delta_{LT}}{E_0 - E}\right)^{-1}\right], \tag{2.13}$$

in which the coefficients A_1, A_2 were expressed in terms of exciton parameters

$$A_1 = \frac{\varepsilon_0^{1/2}\hbar d \Delta_{LT}}{2cE_0} \Delta E_0, \tag{2.14}$$

$$A_2 = \frac{(2\varepsilon_0)^{1/2}\mu^{3/2} a_{exc}^3 d \Delta_{LT} E_0^2}{4c\hbar^2 E_g^{3/2}} \Delta E_0; \tag{2.15}$$

where Δ_{LT} is the frequency of the longitudinal-transverse splitting; μ is the reduced mass of the electron-hole pair; a_{exc} is the exciton Bohr radius.

The status of the third contribution $\theta_3(E)$ to the Faraday effect is uncertain, since the assumed frequency dependence describes both intracenter transitions in Mn^{2+} ions and higher-energy transitions with $E > E_g$.

3. FARADAY EFFECT IN $A^{II}B^{VI}\langle Mn\rangle$ AND $A^{II}_{1-x}Mn_xB^{VI}$ SEMICONDUCTORS: ANOMALIES IN SPECTRAL, CONCENTRATION, TEMPERATURE, AND MAGNETIC FIELD DEPENDENCES

Let us now turn to the experimental results on the Faraday effect in SMS. The sharp enhancement of FR was first

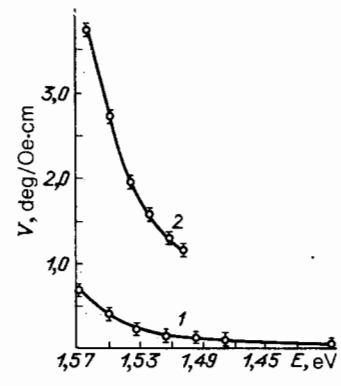

FIG. 2. Spectral dependence of the Verdet constant at $T = 1.7$ K in CdTe⟨Mn⟩ samples for various doping levels[1]: $C_{Mn} = 6\times10^{18}$ cm^{-3} (*1*) and 7.2×10^{18} cm^{-3} (*2*).

reported[1] by Komarov *et al.*,[1] who studied CdTe crystals doped with Mn^{2+} ions up to 8.2×10^{18} cm^{-3} concentration. The dispersion of the Verdet constant $V=\theta/Hd$ measured in thin ($d=0.2$ mm) samples with different Mn concentrations at $T=1.7$ K in a magnetic field $H=3.65$ kOe is shown in Fig. 2. The sharp rise in $V(E)$ coincides with the absorption edge of the crystal or, more precisely, with the long-wavelength tail of the main exciton band; the FR efficiency increases with the doping level. The authors of Ref. 1 also demonstrated that the magnetic field dependence of the FR angle saturates at high fields. They investigated the nature of the observed FR effects by pump-exciting the samples at microwave frequencies and observed a sharp decrease of FR at fields corresponding to the electron paramagnetic resonance (EPR) of Mn^{2+} ions in cadmium telluride. This made it possible to relate uniquely the observed Faraday effect enhancement in CdTe⟨Mn⟩ to the spin polarization of Mn^{2+} impurity ions. Direct spectroscopic observation of large exciton band splitting in magnetic fields indicates that the Faraday effect is due to the splitting of the exciton band into σ^+ and σ^- components. The magnitude of this splitting, like the extent of FR enhancement, is determined not by the external magnetic field itself, but rather by the field-induced magnetization of the paramagnetic Mn^{2+} ion subsystem in CdTe. Apparently this is the case for the entire $A^{II}B^{VI}$⟨Mn⟩ semiconductor family. Thus, for example, Gubarev[21] studied manganese-doped cadmium sulfide crystals and observed a severalfold enhancement of FR over the undoped crystal value, with the magnetic field dependence tending towards saturation (Fig. 3). The form of this field dependence is well approximated by the Brillouin function $B_{5/2}(\mu_B gH/kT)$, which describes the Boltzmann distribution of a spin 5/2 system over the Zeeman components.

We should note that at helium temperatures the absorption edge spectrum of hexagonal cadmium sulfide crystals is dominated by A-, B-, and C-exciton transitions and consequently the FR spectrum is largely determined by the spin-splitting of the lowest-lying (A-exciton) resonance.

The above-described measurements on doped semiconductors demonstrated that the magnitude of the Verdet constant depends strongly on the magnetic ion concentration. Accordingly, a markedly greater FR enhancement should occur in solid solutions containing a magnetic component. To date the most detailed investigations of the Faraday effect in solid solutions have focused on the $Cd_{1-x}Mn_xTe$ system. The giant FR effect in solutions with Mn concentration $x\leqslant0.5$ was first reported by Gaj and co-workers.[2] Their results indicate (Fig. 4) that the Verdet constant of $Cd_{1-x}Mn_xTe$ is at least an order of magnitude larger than of pure CdTe crystals. The actual value of the constant varies strongly with temperature and x, while the spectral dependence $V(E)$ deviates from the spectrum of the interband Faraday effect observed in nonmagnetic semiconductors. Originally, Gaj *et al.* presented[2] the data on the FR spectrum of $Cd_{1-x}Mn_xTe$ in a particularly simple fashion: all experimental curves for various values of T and x, plotted on a logarithmic scale, could be mapped onto each other by vertical and horizontal translation. This could be taken as evidence for the generality of the physical mechanisms underlying the Faraday effect at different T and x values. Yet subsequent measurements yielded more complex spectral dependences of FR. In particular, Gaj[22] was the first to note that FR in $Cd_{1-x}Mn_xTe$ is opposite in sign to FR in CdTe. A more thorough analysis of the complex FR dispersion at various T and x values was carried out in Refs. 14, 17–19, 80.

It follows from Fig. 5 that, at room temperature, as the concentration x is increased and we go from "pure" CdTe to $Cd_{1-x}Mn_xTe$ solutions, not only does the FR angle increase, but it also changes sign. Moreover, in samples with $x=0.01$ the sign of FR changes depending on photon energy E. Note that near $E\approx1.47$ eV ($\lambda\approx0.85\,\mu$m) the Verdet constant is independent of Mn concentration in the $0.05\leqslant x\leqslant0.3$ range. If, instead, the sample composition is fixed, similarly complicated FR dispersion is observed as a function of temperature. For instance, if $x=0.007$, the sign reversal of FR observed at $T=300$ K disappears if the temperature is either increased or decreased (Fig. 6). Note that analogous concentration and temperature FR behavior was observed[14] in $Zn_{1-x}Mn_xTe$ solutions (Figs. 7, 8), but there the sign reversal of the FR angle occurs at a higher Mn content $x=0.05$.

Apparently, the observed anomalies in the spectral dependence of FR are common to the entire SMS class of $A^{II}{}_{1-x}Mn_xB^{VI}$. They indicate that FR in SMS is determined by several mechanisms whose relative contributions can vary strongly (both in magnitude and sign) with tempera-

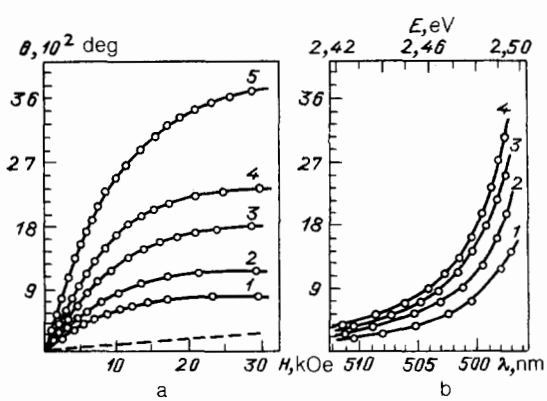

FIG. 3. Faraday rotation angle in CdS⟨Mn⟩ crystals as functions of magnetic field (a) for various wavelengths (λ (nm) = 505 (*1*); 502.5 (*2*); 500 (*3*); 498.5 (*4*); 496.5 (*5*)) and of wavelength (b) for various magnetic fields (H (kOe) = 5.2 (*1*); 8.6 (*2*); 14.7 (*3*); and 47.5 (*4*)) taken from Ref. 21. Other experimental parameters: $T=1.75$ K; $d=1$ mm; $C_{Mn}=2.2\times10^{19}$ cm^{-3}. Dashed line–$\theta(H)$ for nominally undoped CdS at $\lambda=496.5$ nm.

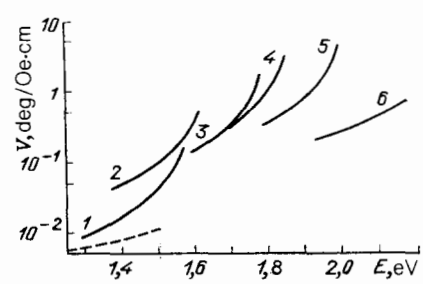

FIG. 4. FR spectra of $Cd_{1-x}Mn_xTe$ crystals at $T=77$ K for various compositions: $x=0.02$ (*1*), 0.05 (*2*), 0.15 (*3*), 0.2 (*4*), 0.3 (*5*), and 0.5 (*6*), taken from Ref. 2. Dashed line–Fr in CdTe.

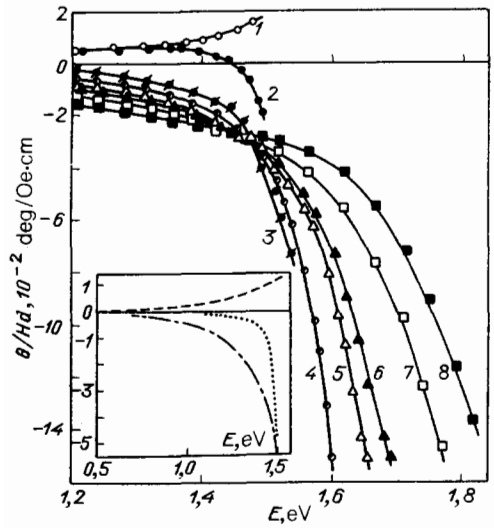

FIG. 5. Spectral dependence of FR for various $Cd_{1-x}Mn_xTe$ crystal compositions at $T = 300$ K (Ref. 17): $x = 0$ (*1*), 0.007 (*2*), 0.05 (*3*), 0.1 (*4*), 0.15 (*5*), 0.2 (*6*), 0.25 (*7*), and 0.3 (*8*). The lines in the inset show the qualitative behavior of the negative $\theta_1(E)$ (dash-dotted) and $\theta_2(E)$ (dotted) contributions together with the positive $\theta_3(E)$ contribution (dashed) for $x = 0.007$, $E_g = 1.52$ eV, $E_0 = 1.51$ eV, and $E_{eff} = 2.43$ eV.

ture and Mn concentration. Some of these mechanisms, involving interband (θ_1), exciton (θ_2), and intracenter (θ_3) transitions in SMS, were already mentioned in Section 2.

In order to analyze the temperature dependence of the Faraday effect in SMS we will follow Ref. 14 and factor out an explicitly temperature-dependent coefficient D in formula (2.9):

$$D = \frac{35}{12}\frac{F_0^{1/2}}{2\hbar c}\frac{g_{Mn}\mu_B N_0 (J_h - J_e)\, x^*}{k\,(T + T_{AF})}. \tag{3.1}$$

where x^* is the effective Mn concentration. Since $\theta(T) \sim D(T) \sim T^{-1}$, the temperature dependence of D^{-1}

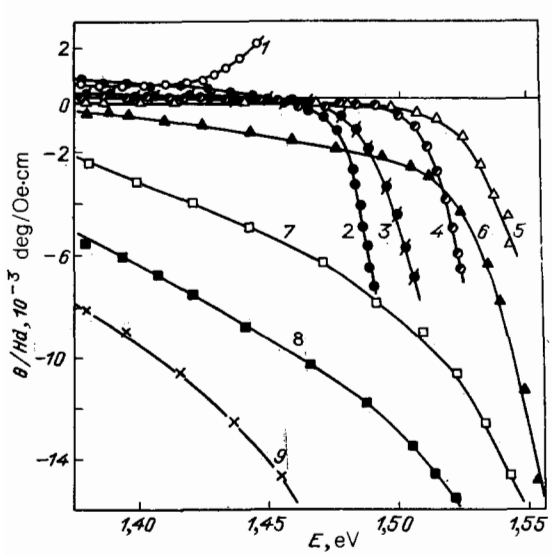

FIG. 6. FR spectra for $Cd_{0.993}Mn_{0.007}Te$ crystals at various temperatures (Ref. 17): T (K) = 350 (*1*), 270 (*2*), 230 (*3*), 200 (*4*), 140 (*5*), 85 (*6*), 20 (*7*), 12 (*8*), and 4.2 (*9*).

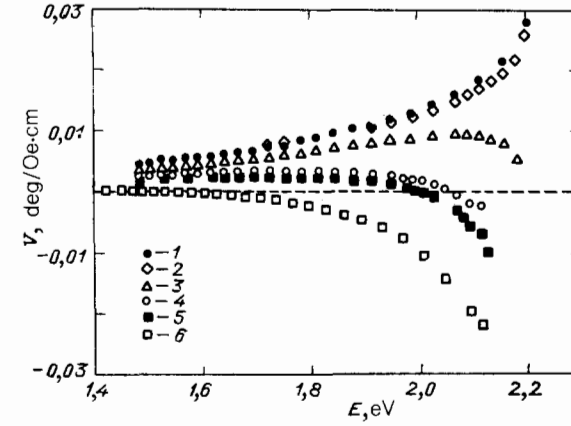

FIG. 7. FR spectra for $Zn_{1-x}Mn_xTe$ crystals of various compositions at $T = 300$ K (Ref. 14): $x = 0$ (*1*), 0.003 (*2*), 0.02 (*3*), 0.05 (*4, 5*) and 0.1 (*6*).

must be linear

$$D^{-1} = m\,(T + T_{AF}), \tag{3.2}$$

where T_{AF} is an empirical parameter and m is the slope of the straight line $D^{-1} = f(T)$.

Experimental data shown in Fig. 9 demonstrate that $D^{-1}(T)$ is indeed linear in the $T \leqslant 40$ K range. An analogous approximation for the temperature dependence of FR in $Cd_{1-x}Mn_xTe$ crystals of various compositions allows for a simple comparison of the parameters m and T_{AF}. This comparison is summarized in Table I. Clearly T_{AF} increases with x, indicating the increased probability of antiferromagnetic pairing of Mn^{2+} ions. At the same time, this extrapolation cannot account for compositions with $x \geqslant 0.45$, which undergo a paramagnetic–spin glass transition. Recall also that for $x \approx 0.7$ magnetic ordering occurs at $T = 40$ K.

The magnetic field dependence of FR in SMS also reflects exchange interaction processes between Mn^{2+} ions. We have already noted that in magnetically doped crystals, the field dependence of the FR angle in SMS saturates at high fields because of the complete alignment of Mn^{2+} spins

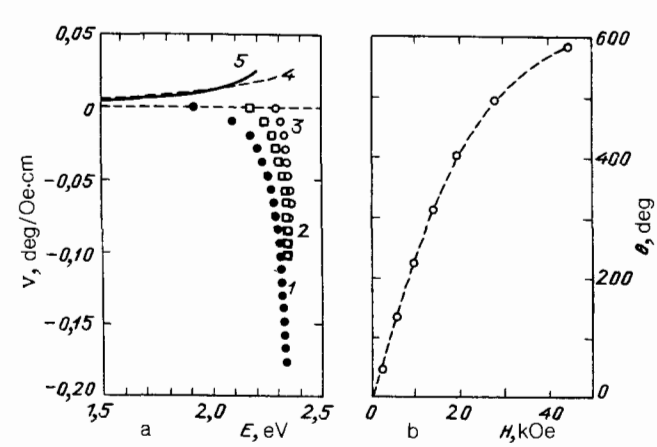

FIG. 8. Verdet constant of $Zn_{0.007}Mn_{0.003}Te$ as a function of photon energy (a) and magnetic field intensity (b) (Ref. 14): T (K) = 5 (*1*), 10 (*2*), 20 (*3*), 77 (*4*), and 300 (*5*). In (b) $E = 2.29$ eV, $T = 5$ K, $d = 2.4$ mm.

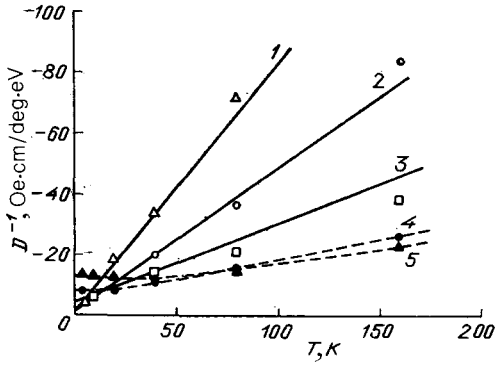

FIG. 9. Temperature dependence of parameter D in $Cd_{1-x}Mn_xTe$ crystals of various compositions[14]: $x = 0.05$ (*1*), 0.1 (*2*), 0.35 (*3*), 0.45 (*4*), and 0.70 (*5*).

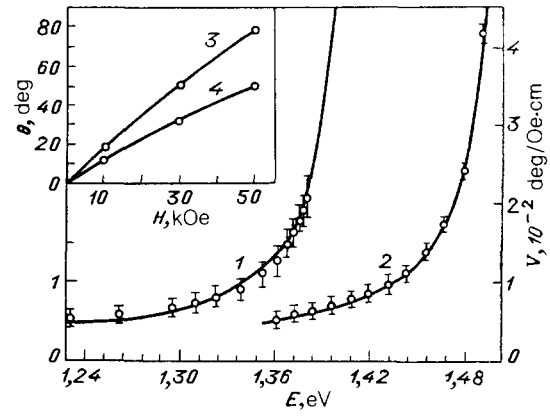

FIG. 10. Spectral dependence of the Verdet constant in GaAs⟨Mn⟩ with $C_{Mn} = 5\times10^{18}$ cm^{-3} at $T = 2$ K (*1*) and 300 K (*2*) (Ref. 30). Inset shows the magnetic field dependence of FR at $T = 2$ K, $E = 1.463$ eV (*3*) and $E = 1.426$ eV (*4*).

(in Fig. 8, *b* this effect is illustrated in $Zn_{1-x}Mn_xTe$). Such behavior of $\theta(H)$ would be expected if one ignored the interaction between Mn^{2+} ions. On the other hand, the use of strong pulsed magnetic fields of up to 250 kOe revealed that the FR field dependence in $Cd_{0.95}Mn_{0.05}Te$ crystals continues to rise monotonically with H.[17] According to the authors of Ref. 17, this increase in $\theta(H)$ is related to the steps in the magnetization $\langle S_z\rangle$ of the magnetic subsystem in SMS. This step-like behavior of $\langle S_z\rangle(H)$, in turn, is due to the appearance of magnetic ion clusters in SMS–as the external field increases these clusters dissociate, resulting in separated, noninteracting ions.

We should note that there has been much recent discussion[23-27] of the possibility of explaining the $\langle S_z\rangle(H)$ dependence in SMS with small x in terms of the antiferromagnetic interaction between nearest-neighbor ions in Mn^{2+}–Mn^{2+} pairs only. In these papers the Mn^{2+} ions were assumed to be randomly distributed over the cation sites of the crystalline lattice. Then, the appearance of 5 steps in the high-field magnetization of the crystals can be attributed to the crossing of the energy levels of the Mn^{2+}–Mn^{2+} pair as H increases. Other types of exchange interactions (for example, the dissociation of clusters consisting of three, four, or more Mn^{2+} ions) are assumed to be negligibly small. This picture fully accounts for the recently reported observation of step-like changes of FR in $Cd_{1-x}Mn_xTe$ crystals as H is increased.[28] Evidently, the observation of step-like characteristics in the FR magnetic field dependence enhances the methodological possibilities of utilizing the Faraday effect to determine the exchange interaction constants in magnetic ions. This is important for the theory of exchange interactions in SMS and clearly complements such well-tested techniques as the direct measurement of magnetization $\langle S_z\rangle(H)$ or of the field-induced spin splitting of the excitonic states $\Delta E_0(H)$.

One of the necessary conditions for observing the steps in $\theta(H)$ is the sufficiently low temperature ($T\approx4$ K) required to minimize thermal broadening of energy levels. Yet we should also mention an interesting effect observed at room temperature in ultra-strong magnetic fields of up to 1500 kOe: the Verdet constant of $Cd_{1-x}Mn_xTe$ increases nonlinearly with magnetic field.[29] Further study is required to elucidate the mechanism responsible for this effect.

4. THE FARADAY EFFECT IN OTHER SMS

The obvious question that arose after the discovery of exchange interaction effects in $A^{II}B^{VI}\langle Mn\rangle$ and $A^{II}{}_{1-x}Mn_xB^{VI}$ type SMS was whether giant FR could be observed in other semiconductors that contain magnetic ions but have a basic matrix other than the $A^{II}B^{VI}$ group. Reports of such investigations have recently begun appearing in the literature.

4.1. GaAs⟨Mn⟩

Strong FR near the fundamental absorption edge has been observed in GaAs, a group $A^{III}B^{V}$ semiconductor, doped with Mn up to $C_{Mn} = 5\times10^{18}$ cm^{-3} (Fig. 10).[30] Still, the magnitude of GaAs⟨Mn⟩ FR was much smaller than the CdTe⟨Mn⟩ value (compare with Fig. 2). The sign of FR in GaAs⟨Mn⟩ is the same as in undoped GaAs. The spectral dependence of the Faraday effect in GaAs⟨Mn⟩ is temperature-invariant, shifting only to follow the temperature-induced change in the bandgap. Further, the magnetic field dependence of FR in this material is nearly linear with field (see inset of Fig. 10). Evidently the properties of FR in GaAs⟨Mn⟩ are determined by the *s–d* exchange interactions

TABLE I. Parameters in the function $D^{-1}(T)$ for $Cd_{1-x}Mn_xTe$ (Ref. 14).

Composition x	m, Oe·cm/deg·eV·K	T_{AF}, K	Composition x	m, Oe·cm/deg·eV·K	T_{AF}, K
0,05	—0,829	1,0	0,23	—0,352	7,3
0,10	—0,468	3,3	0,35	—0,261	15,2

between Mn^{3+} ($3d^4$) ions and band carriers, as well as by Van Vleck paramagnetism of manganese ions. An indirect confirmation of this picture is the absence of EPR in GaAs⟨Mn⟩ crystals.[30]

$A^{III}B^{V}$ solid solutions with magnetic components have not been studied because the solubility of transition metals in the matrix of $A^{III}B^{V}$ crystals is low.[31,32]

4.2. CdP_2 ⟨Mn⟩

Abramishvili and co-workers[33] investigated FR in Mn-doped CdP_2 crystals. Their results are shown in Fig. 11. We see that doping the crystal with Mn leads to rather small changes in the spectral dependence of FR and does not alter its sign. At the same time, the field dependence of FR becomes markedly nonlinear at high magnetic fields and can be approximated by the Brillouin function for a spin 5/2 system. This behavior corresponds to the magnetization of the Mn^{2+} ion spin system, suggesting that the effect of Mn^{2+} ions on the magnetooptic characteristics of CdP_2 is not related to the carrier-impurity exchange interaction affecting the energy structure and electronic transitions of the matrix, but rather to the direct contribution of electronic transitions within Mn^{2+} ionic shells.[33] The spectral range shown in Fig. 11 is close to the intracenter $^6A_1$ (^6S) → $^4T_1$ (^4G) transition frequency in Mn^{2+}; the low symmetry of the CdP_2 crystal makes these transitions more probable.

As for the weakness of carrier-impurity exchange interactions in CdP_2 ⟨Mn⟩, there are two explanations: the relatively small values of the exchange integrals in comparison with $A^{II}B^{VI}$⟨Mn⟩ systems and the large carrier scattering by the Mn^{2+} impurity ionic potentials in CdP_2.

4.3. $Pb_{1-x}Mn_xI_2$

Solid solutions in the PbI_2–MnI_2 system provided another class of SMS that exhibited giant enhancement of the interband Faraday effect due to the magnetic component. This enhancement has been attributed to the exchange interaction between photoexcited carriers and localized Mn^{2+} ionic spins.[20,34]

The binary PbI_2 and MnI_2 compounds have layered crystalline lattices (D_{3d} symmetry group) characterized by hexagonal close packing of I^- anions. The Pb^{2+} and Mn^{2+} cations are located in the octahedral spaces between adjacent iodide layers. The similarity of PbI_2 and MnI_2 crystal lattices and the closeness of lattice parameters promotes the formation of PbI_2–MnI_2 solid solutions.[35] The formation of $Pb_{1-x}Mn_xI_2$ solid solutions in the $0 \leqslant x \leqslant 0.15$ range has been confirmed by excitonic reflection, absorption, and photoluminescence spectra.[36–39] We should note that these measurements revealed a strong compositional dependence of the spectra, with the exciton structure shifting towards shorter wavelengths and broadening with increasing Mn content (as Mn replaces Pb). As in $A^{II}{}_{1-x}Mn_xB^{VI}$ crystals, the compositional dependence of the exciton energy in $Pb_{1-x}Mn_xI_2$ is linear, with the dE_0/dx coefficient being 1.25 ± 0.05 eV.[36]

The spectral dependence of FR for several compositions of $Pb_{1-x}Mn_xI_2$ is shown in Fig. 12.[20] Clearly, FR in $Pb_{1-x}Mn_xI_2$ is opposite in sign and markedly larger in magnitude than in the binary PbI_2 compound. Analogously to the $A^{II}{}_{1-x}Mn_xB^{VI}$ crystals, the FR in $Pb_{1-x}Mn_xI_2$ can be adequately described by the excitonic contribution $\theta_2(E)$ (2.13) as long as the detuning $\Delta E = E_0 - E$ is small. At larger values of ΔE the interband $\theta_1(E)$ contribution (2.12) should be taken into account. In Fig. 12 we see that calculated and experimental results for $Pb_{1-x}Mn_xI_2$ crystals with $x = 0$ and $x = 0.01$ are in good agreement, whereas in $x = 0.03$ crystals there is a discrepancy at small ΔE (this is

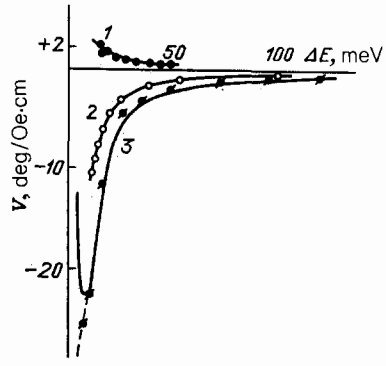

FIG. 12. Faraday rotation in $Pb_{1-x}Mn_xI_2$ as a function of detuning ΔE at $T = 2$ K.[20] Markers adjacent to curves *1–3* are experimental values for $x = 0$, 0.01, and 0.03, respectively; curves *1–3* are calculated from (2.11).

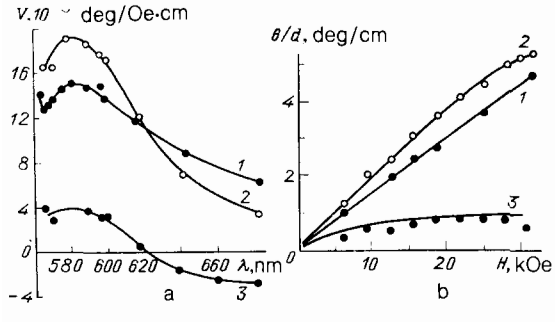

FIG. 11. Spectral (a) and magnetic field (b) dependence of FR in CdP_2 (*1*) and CdP_2 ⟨Mn⟩ (*2*) crystals. Curve *3* is the difference between curves *2* and *1* (Ref. 33).

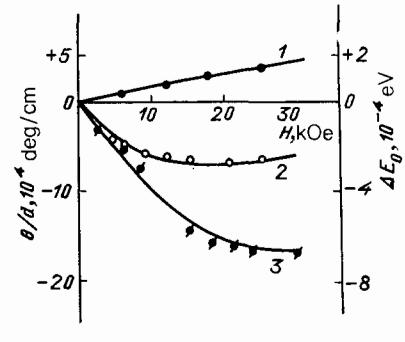

FIG. 13. FR and ΔE as functions of the magnetic field in $Pb_{1-x}Mn_xI_2$.[20] Markers adjacent to curves *1–3* are experimental values for $x = 0$, 0.01, and 0.03 obtained at $E = 2.495$, 2.516, and 2.466 eV, respectively. Line *1* connects the points, curves *2* and *3* represent the difference of contributions proportional to the Brillouin function and that given by the straight line *1*.

due to inhomogeneous broadening; if the latter is taken into account the discrepancy disappears).

The magnetic field dependences of FR, $\theta/d(H)$, and of calculated spin splittings, $\Delta E_0(H)$, are shown in Fig. 13. The spin splittings were calculated from expressions (2.13) and (2.15) that relate ΔE_0 to θ. Unlike pure PbI_2, $Pb_{1-x}Mn_xI_2$ exhibits nonlinear $\theta(H)$ and $\Delta E_0(H)$ that can be approximated by the difference between the Brillouin function and the linear Zeeman contributions. Saturation and even tendency towards possible reduction of $\theta(H)$ indicates that these contributions are comparable at small x and high magnetic fields.

The enhancement of the Faraday effect can also be evaluated in terms of the g^*, the effective g-factor (at low fields where $\langle S_z \rangle$ is proportional to H), or the sum of exchange constants. Proceeding from the calculated values of ΔE_0, Abramishvili and co-workers[20] obtained $g^* = -15 \pm 6$ and $N_0(J_e + J_h) \sim -0.04 \mp 0.02$ eV. The latter quantity is significantly smaller than the sum of the exchange constants in $A^{II}{}_{1-x}Mn_xB^{VI}$, even though the considerable enhancement of the Faraday effect in $Pb_{1-x}Mn_xI_2$ indicates that the exchange splitting of the energy bands is quite significant in these crystals.

The analogy between $Pb_{1-x}Mn_xI_2$ and $Cd_{1-x}Mn_xTe$ extends to the sign reversal of the FR angle as a function of Mn content and temperature.[40] Hence, in addition to the exciton and interband terms, the positive third contribution $\theta_3(E)$ to the FR should probably be considered in $Pb_{1-x}Mn_xI_2$. However, as the exchange constants in $Pb_{1-x}Mn_xI_2$ are smaller than in $Cd_{1-x}Mn_xTe$, the contributions of the first two terms to the total FR become dominant only at lower temperatures. Moreover, in $Pb_{1-x}Mn_xI_2$ the contribution of ionic transitions in Mn^{2+} can be greater because of the larger bandgap E_g, since the intracenter transitions now fall into the transparent region of the semiconductor.

We should note that the layered structure of $Pb_{1-x}Mn_xI_2$ crystals makes it possible to fabricate thin samples appropriate for measuring the Faraday effect in the immediate vicinity of the exciton transition region.[41] In thin samples ($d \approx 1$ μm), as the magnetic field in increased the spectral dependence of FR exhibits a clear dip on top of the positive peak (Fig. 14). This dip can be attributed to the Zeeman splitting of the absorption line when the doublet components are of equal intensity.

We can summarize the experimental results on the Faraday effect in various SMS materials as follows:

–the giant Faraday effect, caused by exchange interactions of excitons and carriers with magnetic ions, is most pronounced in $A^{II}B^{VI}\langle Mn\rangle$ and $A^{II}{}_{1-x}Mn_xB^{VI}$ semiconductors;

–among other SMS, only $Pb_{1-x}Mn_xI_2$ solid solution crystals exhibit Faraday behavior analogous to the $A^{II}{}_{1-x}Mn_xB^{VI}$ system, despite a markedly smaller sum of exchange constants that characterize the carrier-ion exchange interactions;

–in some SMS the complicated character of FR spectra with concentration and temperature-dependent sign reversal of the rotation angle is due to the competition of three different mechanisms (exciton, interband, and intracenter transitions) contributing to the Faraday effect.

5. FARADAY ROTATION (FR) AND THE PARAMAGNETIC–SPIN GLASS PHASE TRANSITION

Faraday effect measurements have also proved effective in the study of the paramagnetic–spin glass transition in SMS. These measurements are sensitive to the magnetic and cooling history of the sample. Thus, for example, in Ref. 42 Faraday effect measurements were carried out in the following regime. The $Cd_{1-x}Mn_xTe$ sample was cooled from $T > 50$ K to $T \leqslant 4$ K in zero magnetic field. After the sample reached base temperature the external field was switched on and FR was measured in a constant magnetic field as temperature was increased from 4 to 50 K. The sample was then cooled back down to 4 K in the magnetic field. We see from Fig. 15 that FR increases with temperature until $T = T_1$, remains constant for $T_1 < T < T_2$, and then decreases with temperature for $T > T_2$. When $\theta(T)$ is subsequently measured as the temperature is decreased in a magnetic field, FR agrees with the original curve down to $T = T_1$, but then deviates for $T < T_1$. It has been demonstrated that the critical

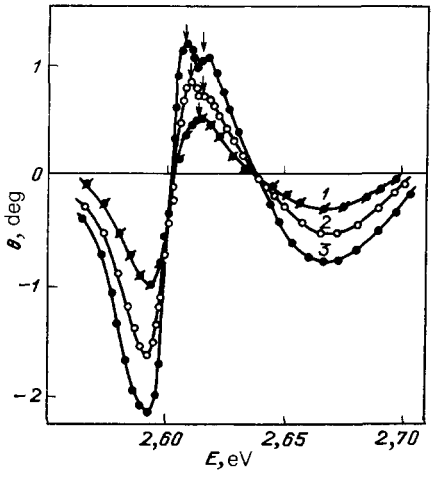

FIG. 14. FR dispersion in $Pb_{0.92}Mn_{0.08}I_2$ at $T = 5$ K (Ref. 41): H (kOe) = 5 (*1*), 15 (*2*), and 20 (*3*).

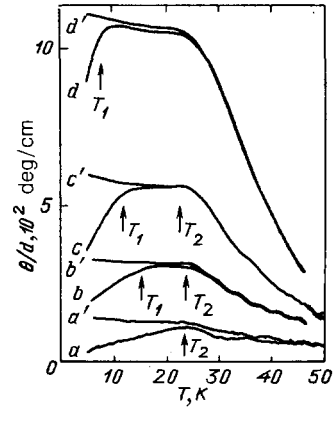

FIG. 15. Temperature dependence of FR in $Cd_{0.45}Mn_{0.55}Te$ crystals.[42] Curves *a–d* are measured after cooling the sample in zero magnetic field and then increasing T in fields of $H = 3$, 10, 20, and 60 kOe, respectively; curves *a'–d'* are measured by cooling the samples in the magnetic field.

temperatures T_1 and T_2 depend on the external field; at H close to zero T_1 and T_2 coincide.

An analysis of these results leads to the conclusion that the $Cd_{1-x}Mn_xTe$ solid solution system remains a spin glass at $T < T_1$ even in a strong magnetic field. In this temperature regime, raising T only reorients the cluster magnetization with respect to the magnetic field direction. In the next temperature regime, $T_1 < T < T_2$, the magnetic moments of all clusters are aligned and the system resembles the spin-flop phase of a weakly anisotropic antiferromagnet in a strong field. The analogy with the spin-flop antiferromagnetic phase is supported by the fact that the temperature dependence of magnetization $\langle S_z \rangle$ has a plateau when $T_1 < T < T_2$, just as in an antiferromagnet the transverse susceptibility is practically independent of T for $T < T_N$ (T_N being the Neel temperature). When the temperature reaches T_2, thermal fluctuations finally destroy the ordering of transverse components, and for $T > T_2$ the $Cd_{1-x}Mn_xTe$ crystal is paramagnetic.

A somewhat different FR behavior with alternating temperature changes near the phase transition point was observed in weak magnetic field experiments (Fig. 16).[43,44] Interestingly, the peak in $\theta(T)$ becomes weaker in repeated measurements. Other authors[45,46] observed only a change in slope of the FR temperature dependence in $Hg_{1-x}Mn_xTe$ crystals, while in the quaternary solid solutions $Hg_{1-y-x}Mn_yCd_xTe$ the spin glass transition occurred at lower temperatures. Furthermore, the following tendency was noted: if the Mn content is held fixed, the "cooling" temperature in SMS decreases as the bandgap E_g increases. Apparently, the long-range antiferromagnetic interaction between Mn^{2+} ions mediated by virtual transitions between valence and conduction bands plays an important role in the mechanism responsible for spin glass formation in SMS.

Faraday rotation measurements have been successfully employed to determine the real χ' and imaginary χ'' components of SMS magnetic susceptibility in the temperature range corresponding to spin glass formation.[47-56] Experimental results obtained[47,48] for $Hg_{1-x}Mn_xTe$ in the $70 \leqslant \nu \leqslant 3000$ Hz frequency range are adequately described by a simple phenomenological model based on a wide distribution of relaxation times. The temperature dependence of magnetic susceptibility components χ' and χ'' at $\nu = 272$ Hz in $Hg_{0.7}Mn_{0.3}Te$ is shown in Fig. 17. The $\chi'(T)$ contains a peak at the "cooling" temperature $T = 9.2$ K. The behavior of $\chi'(T)$ and $\chi''(T)$ is similar to that of many spin glass systems. The similarity extends to the frequency dependence of the peak in $\chi'(T)$, which shifts towards higher temperatures as the frequency is increased.

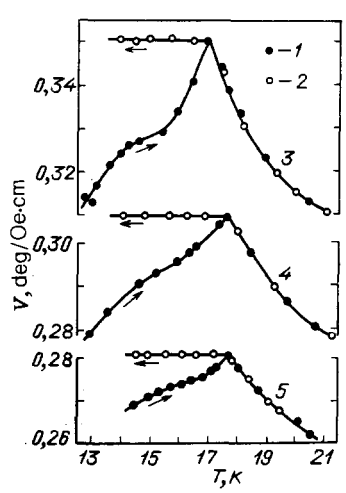

FIG. 16. Temperature dependence of FR in $Cd_{0.5}Mn_{0.5}Te$ crystals near the spin glass transition region.[44] Markers *1* correspond to cooling at $H = 0$, *2*–cooling at $H \neq 0$. The curves correspond to H (Oe) = 20 (*3*), 50 (*4*), and 350 (*5*).

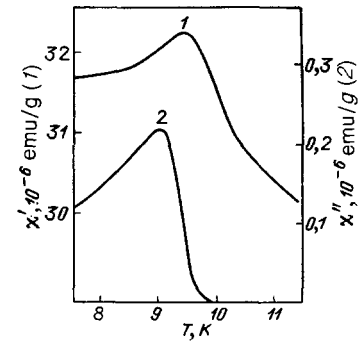

FIG. 17. Temperature dependence of χ' (*1*) and χ'' (*2*) magnetic susceptibility components in $Hg_{0.7}Mn_{0.3}Te$ (Ref. 47), for $H = 51$ Oe, $\nu = 272$ Hz.

If the spin glass is described as an aggregate of magnetic formations with a wide spectrum of relaxation times $q(\tau)$, the components χ' and χ'' can be written as follows:[47]

$$\chi' = \frac{1}{H} \int_{\tau_{min}}^{\tau_{max}} \frac{M(\tau)}{1+\omega^2\tau^2} q(\tau)\, d\ln\tau, \tag{5.1}$$

$$\chi'' = \frac{1}{H} \int_{\tau_{min}}^{\tau_{max}} \frac{M(\tau)\,\omega\tau}{1+\omega^2\tau^2} q(\tau)\, d\ln\tau, \tag{5.2}$$

where τ_{min}, τ_{max} are the shortest and longest relaxation times in the system. According to the model of Ref. 51, if $\tau_{max} \ll \omega^{-1}$ the system is paramagnetic, while $\tau_{min} \ll \omega^{-1} \ll \tau_{max}$ corresponds to a spin glass.

The FR measurement technique has been used to construct the magnetic phase diagram of $Hg_{1-x}Mn_xTe$. For $x > 0.25$ the compositional dependence of the transition temperature T_s is linear, with the extrapolation to intersection with the composition axis giving $x \sim 0.17$. We should point to the adequate agreement between the values of T_s obtained from FR measurements and the other available techniques of constructing the SMS phase diagram. The Faraday effect is clearly a more versatile tool in the study of the spin glass dynamics, however. The theoretically predicted percolation threshold for the formation of an infinite spin cluster is $x_p^{(1)} \approx 0.195$ if only the nearest neighbors are considered, and $x_p^{(2)} \approx 0.136$ if the next-nearest neighbors are also taken into account. The fact that spin glass transitions are observed in $Hg_{1-x}Mn_xTe$ compositions below the percolation thresholds $x_p^{(1)}$ and $x_p^{(2)}$ probably points to the existence of long-range interactions arising via virtual exchange mechanisms.

We should also mention the controversy about the phase transitions in $Cd_{1-x}Mn_xTe$ crystals with large Mn content. Although, as in the above discussion, the peak in $\chi'(T)$ can be interpreted as a signature of the paramagnetic–spin glass transition, Galazka and co-workers[53] have proposed that near $x = 0.7$ the transition could be to an antiferromagnetic state. In their model, the boundaries of the antiferromagnetic and spin glass phases are separated by a multicritical point, such that the spin glass phase can include some concentrations above the percolation threshold. Theoretical investigations of systems with a random spin anisotropy (in higher dimensions) have suggested that both ordered and spin glass phases can be combined in the same magnetic phase diagram.

6. TIME-RESOLVED FR EFFECTS IN SMS

Time-resolved measurements of the Faraday effect in SMS can be nominally grouped into two types. The first type of experiment focuses on temporally long-lived FR effects at temperatures $T < T_s$, i.e., in the spin glass phase. The second type of experiment involves time-resolved measurements with high (picosecond range) resolution.

As we have mentioned earlier, the properties of SMS spin glasses, including the time dependence of the FR angle have been most extensively studied in $Cd_{1-x}Mn_xTe$ crystals.[57,58] Investigations of the spin glass transition employed an FR angle time-resolved measurement procedure analogous to that described above: the sample was cooled in zero magnetic field to some temperature $T < T_s$, a magnetic field $H = 125$ Oe was switched on, and the angle θ was measured at $E = 0.8E_g$ as a function of time t.

Figure 18 shows $\theta(t)$ of $Cd_{0.57}Mn_{0.43}Te$ at several temperatures: $T_1 = 10.2$ K $< T_s$; $T_2 = 11.3$ K $< T_s$; $T_3 = 23$ K $> T_s$. When $T < T_s$ there are clear fluctuations on the slowly increasing $\theta(t)$ background (curves *1*, *2*), whereas for $T > T_s$ the FR angle remains practically constant with time (curve *3*). The fluctuation amplitude reaches 12% of the signal at $t = 1$ min, while the period is approximately 60 min. We should note that the observed fluctuation amplitude at a given temperature T_0 is approximately equal to the difference $(\theta_{FC}(T_0) - \theta_{ZFC}(T_0))$, where $\theta_{FC}(T_0)$ and $\theta_{ZFC}(T_0)$ are, respectively, the temperature dependences of the FR angle for samples cooled in the presence or absence of a magnetic field.

Kierzek–Pecold and co-workers[57,58] have proposed two alternative explanations for the observed time evolution of the Faraday effect in SMS. The first is based on the well-known picture of the energy surface in configuration space, with thermally excited transitions between different energy valleys. The second explanation posits that the nearly periodic fluctuations can be caused by a special type of excitation with a very low intrinsic frequency. We note that no analogous FR fluctuations in the time evolution of magnetization have been observed in spin glass systems other than SMS.

High-resolution time-resolved measurements have been carried out[15] on $Cd_{1-x}Mn_xTe$ crystals with $x = 0.115$ and 0.18 at $T = 1.35$ K. A strong picosecond pulse was applied on top of a constant weak probe. The data acquisition system was tuned to record the effect of this pulse on the intensity of light passing through the polarizer—sample in magnetic field—analyzer system. This set-up consequently measured only the short-lived component of the Faraday effect. The time evolution of the Faraday effect, illustrated in Fig. 19, can be summarized as follows. The signal peaks at the excitation energy $E_{pump} = 1.839$, corresponding to the formation of bound excitons in the semiconductor. The rise time of the signal decreases at higher magnetic fields (see Fig. 19) and with higher Mn content. The total absence of any effect of the pump on FR in "pure" CdTe and $Cd_{1-x}Mn_xTe$ at high temperatures ($T > 10$ K) emphasizes the crucial role of Mn spins in these effects.

It is likely that the time dependence of the magnetization holds the key to the above-described temporal characteristics. The spins of paramagnetic Mn^{2+} ions create some background magnetization $\langle S_z \rangle$, which for $x = 0.18$ is estimated to be $\langle S_z \rangle / S_s = 0.28$ and 0.70 at $H = 10$ and 50 kOe, respectively.

The local polarization of Mn^{2+} ions, caused by the hole-ion exchange, is small compared to this background. The optical pulse creates polarons that lower the local magnetization below the background value.

The creation of acceptor-bound excitons occurs on a time scale of less than 20 ps, while in $Cd_{1-x}Mn_xTe$, for example, their radiative or nonradiative recombination requires $\tau_r \approx 1000$ ps.[15] The rise time of the signal in Fig. 19 is

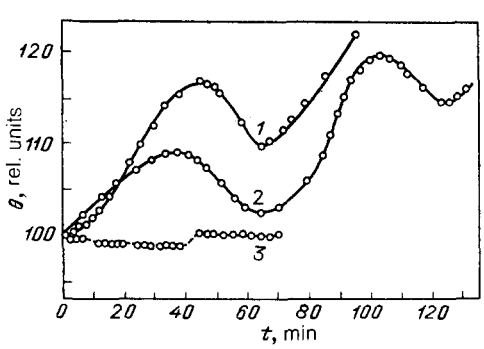

FIG. 18. Time evolution of FR in $Cd_{0.57}Mn_{0.43}Te$ crystals ($T_s = 14$ K) at various temperatures[58]: *1*–$T = 10.2$ K, $H = 50$ Oe; *2*–$T = 11.3$ K, $H = 90$ Oe; *3*–$T = 23$ K, $H = 125$ Oe.

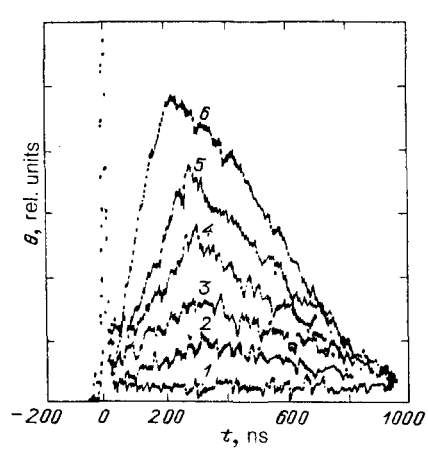

FIG. 19. Time-resolved Faraday effect in $Cd_{0.82}Mn_{0.18}Te$ measured at $E_{pump} = 1.839$ eV, $T = 1.35$ K, and various magnetic fields[15]: H (kOe) = 0 (*1*), 10 (*2*), 20 (*3*), 30 (*4*), 40 (*5*), and 50 (*6*).

consequently determined by the time $\tau_s \approx 400$ ps required for the alignment of Mn^{2+} spins within the exciton Bohr radius, while the decay is governed by the recombination time τ_r.

The initial slope of the signal can be described by the simple dependence

$$\langle S(t)\rangle = (\langle S_z\rangle_0 - \langle S_z\rangle_p)\left(\frac{1}{\tau_s}\right)^{-1}, \tag{6.1}$$

where $\langle S_z\rangle$ is the average magnetization before the optical pulse; $\langle S_z\rangle_p$ is the equilibrium magnetization in the presence of bound excitons.

At $H = 0$ no pump-induced magnetization exists. As H increases the value of $\langle S_z\rangle$ also increases, while $\langle S_z\rangle_p$ remains practically constant. The time τ_s also depends on H and increases in samples with smaller Mn content. At high temperatures thermal fluctuations suppress magnetic interactions and the corresponding $(\langle S_z\rangle - \langle S_z\rangle_p)$ difference term in (6.1) disappears.

7. FREE-CARRIER SPIN-INDUCED FARADAY EFFECT IN $Hg_{1-x}Mn_xTe$

The above-discussed FR measurements on $Hg_{1-x}Mn_xTe$ solid solutions were carried out on samples with large values of x, i.e., compositions with $E_g > 0.5$ eV. Recently, Yuen and co-workers[59] have reported measurements on free-carrier spin-induced FR in narrow-gap $Hg_{1-x}Mn_xTe$.

Since in the absence of a magnetic field the narrow-gap semimagnetic $Hg_{1-x}Mn_xTe$ and nonmagnetic $Hg_{1-x}Cd_xTe$ semiconductors are rather similar, a comparison of the results in these two systems is instructive.

Spin-induced FR in narrow-gap semiconductors with a large effective g-factor and strong spin-photon interaction obeys the following law:[60]

$$\theta = \left(\frac{dS}{d\Omega}\right)_{SF}^{1/2} \frac{dN\lambda\langle S_z\rangle}{n}, \tag{7.1}$$

where the spin-flip Raman scattering cross-section $(dS/d\Omega)_{SF}$ and the coupling constant ξ are defined as follows:

$$\left(\frac{dS}{d\Omega}\right)_{SF} = \frac{4\omega^2\xi}{c^4}, \tag{7.2}$$

$$\xi = \frac{e^2}{2\omega^2 m_s}\frac{E_g E}{E_g^2 - E^2}; \tag{7.3}$$

N is the electron concentration; m_s is the spin quantum number.

Resonant enhancement of ξ for $E \leqslant E_g$ of up to two orders of magnitude has been confirmed in spin-flip Raman scattering experiments.

The spin-induced Faraday effect should saturate at high magnetic fields, when all the spins are aligned $(\langle S_z\rangle = 1)$.

Experimental results (Fig. 20) point to a number of differences between spin-induced FR in $Hg_{0.78}Cd_{0.22}Te$ and $Hg_{0.89}Mn_{0.11}Te$ samples. First of all, the Verdet constant of $Hg_{1-x}Mn_xTe$ is somewhat larger, probably because of a higher g-factor. As the laser intensity increases, so does the FR saturation level in $Hg_{1-x}Cd_xTe$, but in the linear region

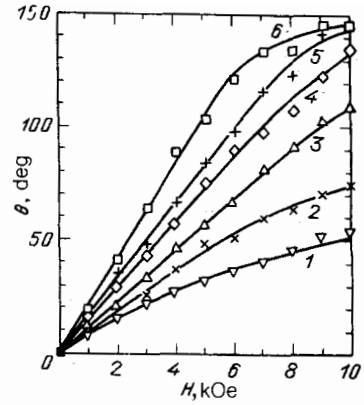

FIG. 20. Magnetic field dependence of FR in n-$Hg_{0.89}Mn_{0.11}Te$ at $\lambda = 9.6$ μm for various laser intensities[59]: I (kW/cm^2) = 1500 (*1*), 241 (*2*), 56 (*3*), 26.7 (*4*), 12.8 (*5*), $\leqslant$5 (*6*).

FR is insensitive to laser intensity. In $Hg_{1-x}Mn_xTe$ SMS, on the other hand, linear FR decreases at higher laser intensities, while the saturation field increases, even though the linear slope is smaller. These discrepancies have been explained by spin-thermal effects. In $Hg_{1-x}Cd_xTe$ the laser beam increases the electron translational energy, but it cannot alter the frozen electron spin positions since spin-flip-scattering events are rare. In SMS, on the contrary, the exchange interaction of carriers and Mn^{2+} ions promotes the rapid transfer of translational energy to the spin system, eventually raising the spin temperature. Complete spin alignment is also impeded by the laser-induced depolarization, leading to the increase of the FR saturation field in $Hg_{1-x}Mn_xTe$ at high laser intensities.

8. LIGHT-INDUCED MAGNETIZATION (INVERSE FARADAY EFFECT) IN $Cd_{1-x}Mn_xTe$ AND $Hg_{1-x}Mn_xTe$

In 1965, Van der Ziel and co-workers[61] discovered that intense, circularly polarized radiation can induce magnetization in some materials. This phenomenon became known as the inverse Faraday effect. It was observed in $CaF_2\langle Eu^{2+}\rangle$ crystals, diamagnetic glasses, and liquids.[62] In SMS materials, light-induced magnetization was observed in $Cd_{1-x}Mn_xTe$[63,64] and $Hg_{1-x}Mn_xTe$.[65] Since these semiconductors exhibit strong exchange interaction between carriers and magnetic ions leading to reciprocal spin orientation, stronger magnetization was expected after irradiation with polarized light.

The first, indirect indications of induced magnetization in SMS were obtained in magnetization measurements[63] on laser-irradiated $Cd_{0.95}Mn_{0.05}Te$. The observed dependence of excitonic luminescence lines on the pump intensity was explained by changes in $\langle S_z\rangle$ caused by exchange scattering of photoexcited carriers by localized Mn^{2+} ionic spin moments.

Subsequently, light-induced magnetization in $Hg_{1-x}Mn_xTe$ was directly observed by Krenn and co-workers.[65] The magnetization was monitored using a pickup coil that was impedance-matched to a SQUID coil. The laser radiation was provided by a CO-laser (E_L = 205–240 meV; 20–100 mW power). The experiments employed a laser beam of fixed intensity whose polarization was modulated

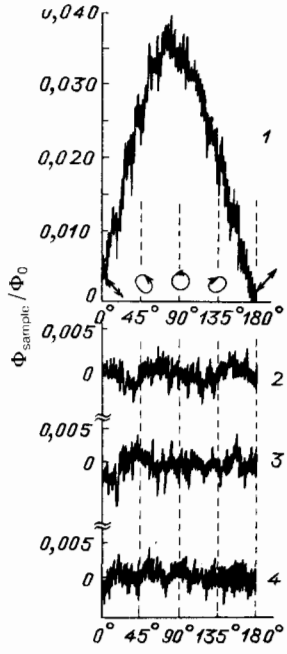

FIG. 21. Magnetic flux measured in a pickup coil proportional to the magnetization of various nonmagnetic and semimagnetic semiconductors as a function of the degree of circular polarization of CO-laser radiation [65]: *1*–$Hg_{0.88}Mn_{0.12}Te$, $E_g = 165$ meV, $E_L = 238$ meV; *2*–$Hg_{0.93}Mn_{0.07}Te$, $E_g = 0$, $E_L = 229$ meV; *3*–$Hg_{0.77}Mn_{0.23}Te$, $E_g = 120$ meV, $E_L = 234$ meV; *4*–InSb, $E_g = 235$ meV, $E_L = 240$ meV.

from linear to circular. Figure 21 shows the measured magnetization as a function of light polarization (in quantum flux units Φ_0). For comparison the data for two compositions of $Hg_{1-x}Mn_xTe$ SMS ($x = 0.07$ and 0.12) are plotted together with data for nonmagnetic $Hg_{1-x}Cd_xTe$ ($x = 0.23$) and InSb semiconductors with approximately the same bandgap E_g. It is evident from Fig. 21 that a signal is recorded only when the $Hg_{1-x}Mn_xTe$ ($x = 0.12$) SMS, which has a finite bandgap, is irradiated with circularly polarized light. No signal is recorded from the zero-gap $Hg_{1-x}Mn_xTe$ ($x = 0.07$) semiconductor, nor from the nonmagnetic $Hg_{1-x}Cd_xTe$ and InSb. The magnetic flux in $Hg_{1-x}Mn_xTe$ SMS increased linearly with laser intensity in the 0.2–1.25 W/cm^2 pump intensity range.

The absence of light-induced magnetization in $Hg_{1-x}Cd_xTe$ and InSb confirms that the inverse Faraday effect in SMS cannot be attributed to spin polarization of electrons and holes. Furthermore, the effect cannot be explained by invoking the direct light-induced polarization of Mn^{2+} ions, for then it would appear in the zero-gap $Hg_{1-x}Mn_xTe$ ($x = 0.07$) as well. Hence, as in the earlier experiments,[63] the dominant mechanism for the appearance of magnetization is the alignment of paramagnetic ions by polarized carriers. In turn, the alignment of localized Mn^{2+} ionic spin moments occurs via spin-flip scattering of polarized free carriers.

As expected, the magnitude of the inverse Faraday effect goes as $1/T$ in the low temperature regime, which is typical of spin relaxation processes involving ion—acoustic phonon interactions.

Recently, light-induced magnetization was investigated in $Cd_{1-x}Mn_xTe$.[64] This series of experiments employed new steady-state and dynamic techniques with picosecond time resolution, making it possible to extract information on the microscopic properties of induced magnetism and its subsequent relaxation.

The experimenters chose $Cd_{0.8}Mn_{0.2}Te$, a material where the bandgap E_g that makes it possible to study dynamical processes at $E > E_g$, $E \approx E_g$, and $E < E_g$. The steady-state dependence of magnetization on E in a sample illuminated with circularly polarized light of fixed intensity is shown in Fig. 22 for two temperatures. Both temperature curves contain three distinct spectral regions. The magnetization is nearly zero at energies where the crystal is transparent, peaks sharply at $E \approx E_g$, and then remains practically constant for $E > E_g$. As in the preceding case of $Hg_{1-x}Mn_xTe$, the magnetization is lower at higher temperatures, but the $Cd_{1-x}Mn_xTe$ system also exhibits some differences. The major of these is the contribution of magnetopolarons to light-induced magnetization. The polarons are due to the strong pairing of carrier and magnetic ion spins and hence have much larger effective moments than the ions themselves. The peaks at photon energies close to E_g in Fig. 22 are due precisely to the formation of magnetopolarons. Although magnetopolarons continue to exist when the photon energy exceeds E_g, their random orientation precludes a large contribution to the magnetization. On the other hand, spin-flip exchange scattering of carriers switches on when $E > E_g$, leading to constant magnetization in this spectral region.

Dynamical studies of $Hg_{0.8}Mn_{0.2}Te$ also suggest that the magnetization response depends on excitation energy. Picosecond magnetization changes in the three aforesaid spectral regions indicate a large disparity in the rise and decay times of the magnetization. A time $t \approx 250$ ps corresponds to polaron formation as determined from the time evolution of the direct Faraday effect.[15] The decay time $t \approx 1000$ ps is typical for carrier recombination in this material. At $E = 1.95$ eV the magnetization is induced almost instantaneously, since the polarization transfer from polarized

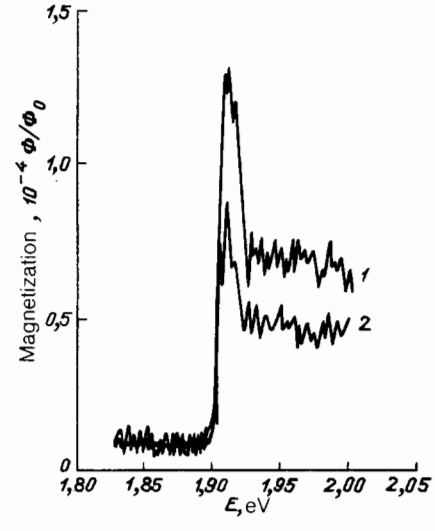

FIG. 22. Induced magnetization in $Cd_{0.8}Mn_{0.2}Te$ as a function of radiation quantum energy at $T = 4.2$ K (*1*) and 5.8 K (*2*) (Ref. 64).

carriers occurs via spin-flip exchange scattering by Mn^{2+} ions on a time scale $t \approx 1$ ps. The decay time of $t \approx 300$ ps observed at this energy probably characterizes the actual spin-lattice relaxation time in this SMS.

The observed light-induced magnetization in SMS is small (of the order of 5×10^{-7} Oe), considerably smaller than expected. This was attributed in Ref. 66 to two effects: a) decrease in magnetization due to magnetic ion-hole interaction; b) strong depolarization of electrons due to their excitation into states above the bottom of the conduction band.

9. FARADAY EFFECT IN THIN SMS FILMS AND SPIN SUPERLATTICES

Many advances in the epitaxial growth of thin semiconductor films have been achieved in recent years. New techniques have also been used to prepare thin SMS films. The properties of the Faraday effect in such films are obviously of considerable interest.

In Ref. 67 $Cd_{1-x}Mn_xTe$ ($0 \leqslant x \leqslant 0.76$) films were obtained by simultaneous evaporation of CdTe and MnTe onto sapphire and glass substrates. The compositional dependence of the bandgap in films evaporated onto sapphire substrates was in adequate agreement with $E_g(x)$ measured in single crystal samples. Also, measurements of the lattice constant demonstrated that $Cd_{1-x}Mn_xTe$ films on sapphire have lattice parameters similar to bulk $Cd_{1-x}Mn_xTe$ crystals, whereas films on glass substrates exhibited considerably larger lattice constants.

Investigations of the Faraday effect in thin films have markedly increased our understanding of SMS processes, above all because the shift towards shorter wavelengths expanded the accessible spectral range. As we have seen in Fig. 23, FR in thin films is dispersive, with sharp extrema and rotation angle sign reversal. The spectral dependence of FR can be related to the absorption spectrum by the Kramers–Kronig relation:

$$\theta(E) = -\frac{E^2}{2\pi} \int_0^\infty \frac{\Delta\alpha(E')/E'}{E'^2 - E^2} dE', \qquad (9.1)$$

where $\Delta\alpha(E')$ is the difference between coefficients for the absorption of right- and left-polarized radiation by a magnetic ion.

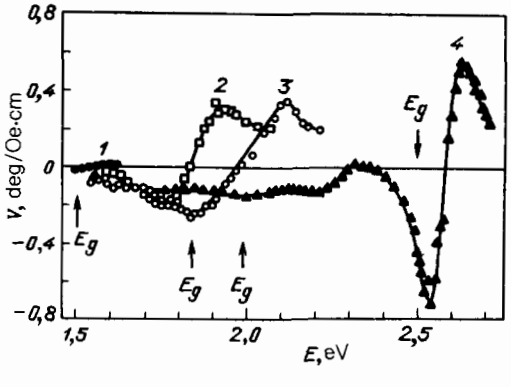

FIG. 23. FR spectra of epitaxial $Cd_{1-x}Mn_xTe$ films of various compositions at $T = 300$ K (Ref. 67): $x = 0$ (*1*), 0.26 (*2*), 0.36 (*3*), and 0.76 (*4*).

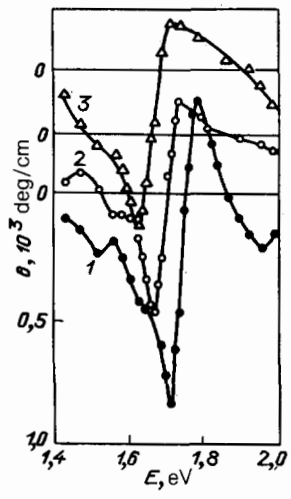

FIG. 24. FR spectra of multilayered $Cd_{0.9}Mn_{0.1}Te$–$Cd_{0.5}Mn_{0.5}Te$ structures with various quantum well widths L (Ref. 70): L (Å) = 40 (*1*), 90 (*2*), and 150 (*3*).

Since SMS are strongly dichroic in a magnetic field (the absorption edge shifts towards longer wavelengths for right-polarized light and towards shorter wavelengths for left-polarized light), equation (9.1) agrees with experiment (Fig. 23). As the Mn content increases, the curves shift towards shorter wavelengths and the extremal values of the Verdet constant increase significantly. Analogous changes in FR curves are observed if $Cd_{1-x}Mn_xTe$ films are cooled. It is likely that the concentration and temperature behavior of $\theta(E)$ can be explained by the same framework of approaches and mechanisms that were previously used to analyze FR data in bulk crystal SMS samples (Section 2). A detailed theoretical study of the Faraday effect in epitaxial $Cd_{1-x}Mn_xTe$ films was recently reported by Koyanagi *et al.*,[68] who took into account the splittings and oscillator strengths of the exciton transitions to second order in perturbation theory.

Modern ion beam epitaxy techniques permit the fabrication not only of thin semiconductor films, but also more complicated, controlled multilayered structures known as superlattices. In the SMS field these structures became known as spin superlattices.[11,69] The FR spectrum for the $Cd_{0.9}Mn_{0.1}Te$–$Cd_{0.5}Mn_{0.5}Te$ spin superlattice[70] is shown in Fig. 24. At first glance the FR dispersion in the spin superlattice appears to follow approximately the sum of FR dispersion curves of the individual $Cd_{0.9}Mn_{0.1}Te$ and $Cd_{0.5}Mn_{0.5}Te$ layers. A detailed analysis reveals the energy position of the main peak amplitude to depend on the superlattice period. This phenomenon is due to the quantum confinement of electrons in a well (layer).

10. APPLICATIONS OF THE FARADAY EFFECT IN SMS

Materials with large Verdet constants have always attracted considerable interest in view of their possible applications in magnetooptic devices. It is not surprising, therefore, that after the discovery of the giant Faraday effect in SMS materials technological research came to supplement purely scientific work.

Table II, compiled from several references[71–73] lists the Verdet constants of the major crystalline and glass-like ma-

TABLE II. Verdet constants of various materials ($\lambda = 633$ nm, $T = 300$ K).

Material	V, rad.$T^{-1}\cdot m^{-1}$	Material	V, rad.$T^{-1}\cdot m^{-1}$
Crystals		Glasses	
$Cd_{1-x}Mn_xTe$	$\leqslant 2000$	M-16 (FR-123)	—71,0
EuF_2	—262	FR-5	—71,—73
$Tb_3Al_5O_{12}$	—180	$Pr(PO_3)_3$	—39,6
$LiTbF_4$	—128	FR-7	—34,9
ZnSe	118	FR-4	—30,5
CeF_3	—114	SF 59	28,5
Bi_4GeO_{12}	29,8	SiO_2	4,0
LaF_3	3,5	SF N64	1,5

terials active in the visible and near IR. Clearly the Verdet constant of $Cd_{1-x}Mn_xTe$ SMS is a record, outdistancing other materials by more than an order of magnitude.

Turner and co-workers[74] analyzed the feasibility of employing $Cd_{1-x}Mn_xTe$ as the active medium for a compact Faraday valve (optical isolator). Recall that these devices are intended for low-loss transmission of radiation in one direction and strong intensity attenuation in the opposite direction.[75]

In addition to the Verdet constant, the relevant characteristics of magnetooptic materials for use as optical isolators are the magnetooptic figure of merit

$$F = \frac{V}{\alpha} \tag{10.1}$$

or the product

$$FH = \frac{\theta}{\alpha d}. \tag{10.2}$$

Table III[56] cites the FH product and the path length in a $Cd_{0.55}Mn_{0.45}Te$ crystal placed in a field $H = 3$ kOe (easily attainable in a permanent magnet) required to rotate the plane of polarization by 45° for light of various wavelengths. It follows from Table III that the required thickness of an optical isolator made of crystalline $Cd_{0.55}Mn_{0.45}Te$ is only ~ 1.3 mm at $\lambda = 633$ nm.

The FR spectral dependence of various $Cd_{1-x}Mn_xTe$ compositions described in Section 3 indicates that in principle these crystals can also be employed in the near IR, particularly at the $\lambda = 1.06\,\mu$m wavelength standard in modern solid state lasers.[81]

Another practical application of the Faraday effect in SMS involves magnetic field sensing. Various groups[18,76–80] have utilized $Cd_{1-x}Mn_xTe$ crystals for this purpose. Butler and co-workers[76–78] have discussed the frequency dependence of the Verdet constant, which is crucial for good dynamic characteristics of magnetic field sensors. Their results indicate reliable device operation at frequencies of several GHz. A schematic diagram of a high-frequency fiber optic field sensor based on SMS is illustrated in Fig. 25. Similarly designed sensors have been combined with visible range lasers, such as He-Ne ($\lambda = 633$ nm) or semiconductor ($\lambda = 670$ nm) lasers, to produce devices with relatively low field detection thresholds of 1 Oe and fairly high frequency ranges ~ 100 MHz.[80] Note, that for $\lambda = 850$ nm, typical of lasers employed in fiber optic technology, the Verdet constant of $Cd_{1-x}Mn_xTe$ is at least an order of magnitude larger than the commonly employed magnetosensitive bismuth silicate and germanate crystals.

Utilization of other SMS materials in fiber optic magnetic field sensors was discussed in Ref. 80. We note here that SMS-based sensors have detection thresholds and sensitivities comparable to sensors based on ferrite garnet films or IYG crystals,[82] but operate over a much wider frequency range.

11. CONCLUSION

The material presented in this review should indicate the wide range of physical problems encountered in studying a well-known physical phenomenon—the Faraday effect—in a new class of materials. Investigations of FR in SMS, as a sub-field of the more general problem of SMS magnetooptics, are far from complete and, in fact, are currently experiencing intensive growth.

We would like to emphasize the methodological advantages of studying the Faraday effect in SMS. Magnetoreflection and magnetoabsorption have often been the techniques of choice in studying exchange interactions in SMS. Yet Faraday spectroscopy has proved more sensitive than direct measurement of Zeeman spin splitting of excitonic and band states, and hence more effective in determining the exchange constants of the interactions of magnetic ions with other magnetic ions and with band carriers. For example, a strong enhancement of the Faraday effect has been observed in $Pb_{1-x}Mn_xI_2$, a new SMS material, at helium temperatures, whereas the exciton line spin splitting has proved difficult to

TABLE III. Magnetooptic parameters of $Cd_{0.55}Mn_{0.45}Te$ crystals ($H = 3$ kOe).

λ, nm	FH, deg/dB	$d = 45°/VH$, cm	λ, nm	FH, deg/dB	$d = 45°/VH$, cm
611,4	16,4	0,068	620,6	65,8	0,096
613,6	22,6	0,079	622,6	94,4	0,104
616,0	34,0	0,082	625,0	158,8	0,109
618,2	46,4	0,087	632,8	464,6	0,131

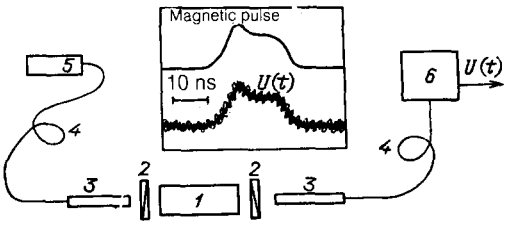

FIG. 25. Schematic diagram of an SMS-based fiber optic magnetic field sensor.[80] *1*–$Cd_{1-x}Mn_xTe$, *2*–polarizers, *3*–lenses, *4*–optical waveguide, *5*–laser, *6*–photodetector.

measure in magnetoreflection[20] or magnetoabsorption[41] spectra.

In a large number of SMS materials the giant Faraday effect is now known to be caused by s, p–d exchange interactions, but we still lack a more rigorous quantitative description of all other mechanisms that can enhance or compensate the main exchange term in FR. In this regard, we should keep in mind the possible contribution of intracenter transitions in magnetic ions, as well as the role of optical transitions between higher-lying states in the Brillouin zone of SMS.

Some SMS have yet to be studied experimentally, including semiconductors doped not only with Mn ions, but with other transition metals of the iron group or with rare-earth elements.

There is hardly any information on the Faraday effect in SMS crystals subjected to electric field or deformation, or a combination of both.

Our understanding of the phase transition problem in SMS is far from complete and the Faraday effect in this regime requires further study.

Investigations of the Faraday effect in thin SMS films and spin superlattices are still in their infancy. Here we can expect to uncover new scientific problems and practical applications. The Faraday effect in SMS will undoubtedly attract the attention of designers of various magnetooptic devices.

The authors of this review hope that it will stimulate additional research in the field of SMS magnetooptics, particularly the Faraday effect in this new class of materials.

[1] A. V. Komarov, S. M. Ryabchenko, O. V. Terletskii, I. I. Zheru, and R. D. Ivanchuk, Zh. Eksp. Teor. Fiz. **73**, 608 (1977) [Sov. Phys. JETP **46**, 318 (1977)].
[2] J. A. Gaj, R. R. Galazka, and M. Nawrocki, Solid State Commun. **25**, 193 (1978).
[3] J. K. Furdyna, J. Appl. Phys. **53**, 7637 (1982).
[4] S. M. Ryabchenko and Yu. G. Semenov, *Spectroscopy of Crystals* (in Russian), Nauka, L., 1983, p. 206.
[5] N. B. Brandt and V. V. Moshchalkov, Adv. Phys. **33**, 193 (1984).
[6] R. R. Galazka, J. Crystal Growth **72**, 364 (1985).
[7] I. I. Lyapilin and I. M. Tsidil'kovskii, Usp. Fiz. Nauk **146**, 35 (1985) [Sov. Phys. Usp. **28**, 349 (1985)].
[8] J. K. Furdyna, J. Vac. Sci. Technol. A **4**, 2002 (1986).
[9] O. Goede and W. Heimbrodt, Phys. Status Solidi b **146**, 11 (1988).
[10] I. Ya. Korenblit and E. F. Shender, Usp. Fiz. Nauk **157**, 267 (1989) [Sov. Phys. Usp. **32**, 139 (1989)].
[11] A. V. Nurmikko, R. L. Gunshor, and L. A. Kolodziejski, IEEE J. Quantum Electron. **QE-22**, 1785 (1986).
[12] M. Faraday, Phil. Mag. **29**, 153 (1846).
[13] F. F. Sizov and Yu. I. Ukhanov, *Magnetooptical Faraday and Voigt Effects in Semiconductors* (in Russian), Naukova dumka, Kiev, 1979.
[14] D. U. Bartholomew, J. K. Furdyna, and A. K. Ramdas, Phys. Rev. B **34**, 6943 (1986).
[15] D. D. Awschalom, J. M. Halbout, S. Molnar, T. Siegrist, and F. Holtzberg, Phys. Rev. Lett. **55**, 1128 (1985).
[16] Yu. G. Semenov, Fiz. Tverd. Tela (Leningrad) **29**, 1908 (1987) [Sov. Phys. Solid State **29**, 1101 (1987)].
[17] P. P. Vatamanyuk, A. V. Savitskii, A. I. Savchuk, and K. S. Ul'yanitskii, Zh. Eksp. Teor. Fiz. **94**, 225 (1988) [Sov. Phys. JETP **67**, 2084 (1988)].
[18] V. I. Konov, P. I. Nikitin, A. M. Prokhorov, A. I. Savchuk, A. V. Savitskii, and K. S. Ul'yanitskii, *Abstracts of Reports at XI All-Union Conf. on Semiconductor Physics* (in Russian), Kishinev, 1988, Vol. 2, p. 170.
[19] D. A. Aksenov, V. I. Konov, P. I. Nikitin, A. M. Prokhorov, A. I. Savchuk, A. V. Savitskii, and K. S. Ul'yanitskii, *Abstracts of Reports at XVIII All-Union Conf. on Physics of Magnetic Phenomena* (in Russian), Kalinin, 1988, Vol. 1, p. 147.
[20] V. G. Abramishvili, A. V. Komarov, S. M. Ryabchenko, B. E. Derkach, and A. I. Savchuk, Fiz. Tverd. Tela (Leningrad) **29**, 1129 (1987) [Sov. Phys. Solid State **29**, 644 (1987)].
[21] S. I. Gubarev, Zh. Eksp. Teor. Fiz. **80**, 1174 (1981) [Sov. Phys. JETP **53**, 601 (1981)].
[22] J. A. Gaj, *Exchange Interaction of Paramagnetic Ions with Band Electrons in $Cd_{1-x}Mn_xTe$* (in Polish), Warsaw Univ. Press, Warsaw, 1981.
[23] R. L. Aggarwal, S. N. Jasperson, P. Becla, and R. R. Galazka, Phys. Rev. B **32**, 5132 (1985).
[24] R. L. Aggarwal, S. N. Jasperson, P. Becla, and J. K. Furdyna, Phys. Rev. B **34**, 5894 (1986).
[25] B. E. Larson, K. S. Haas, and R. L. Aggarwal, Phys. Rev. B **33**, 1789 (1986).
[26] Y. Shapira, S. Foner, P. Becla, D. N. Domingues, M. J. Noughton, and J. S. Brooks, Phys. Rev. B **33**, 356 (1986).
[27] J. P. Lascaray, M. Nawrocki, J. M. Broto, M. Rakoto, and M. Demianiuk, Solid State Commun. **61**, 401 (1987).
[28] A. I. Savchuk, P. I. Nikitin, B. E. Derkach, N. P. Gavaleshko, and Z. N. Smereka, *Abstracts of Reports at IX All-Union Symp. on Spectroscopy of Crystals Activated with Rare-Earth and Transition Metal Ions* (in Russian), Leningrad, 1990, p. 132.
[29] P. Byszewski, M. Z. Cieplak, and M. Romanis, J. Phys. C **12**, 941 (1979).
[30] A. M. Hennel, A. Twardowski, and M. Godlewski, Acta Phys. Polon. A **67**, 313 (1965).
[31] É. M. Omelianovskii and V. I. Fistul, *Transition Metal Impurities in Semiconductors*, A. Hilger, Bristol, Boston, 1986 [Russ. original, Metallurgiya, M., 1983].
[32] V. I. Fistul' (ed.), *Physics and Material Science of Semiconductors with Deep Levels* (in Russian), Metallurgiya, M., 1987.
[33] V. G. Abramishvili, G. I. Bondar', A. V. Komarov, and S. M. Ryabchenko, Ukr. Fiz. Zh. **30**, 1656 (1985).
[34] V. G. Abramishvili, I. V. Blonskii, A. V. Komarov, S. M. Ryabchenko, B. E. Derkach, and A. I. Savchuk, *Abstracts of Reports at XXIV All-Union Conf. on Low-Temperature Physics* (in Russian), Tbilisi, 1986, Vol. 3, p. 22.
[35] V. M. Shmandiĭ and V. K. Miloslavskiĭ, Dep. Ukr. NIINTI 12/16/83, No. 145 UkD84, Kremenchug, 1983.
[36] A. I. Savchuk, B. E. Derkach, and A. N. Lyakhovich, Fiz. Tekh. Poluprovodn. **21**, 1721 (1987) [Sov. Phys. Semicond. **21**, 1041 (1987)].
[37] M. S. Brodin, I. V. Blonskiĭ, V. N. Karataev, B. E. Derkach, and A. I. Savchuk, Fiz. Tverd. Tela (Leningrad) **29**, 1723 (1987) [Sov. Phys. Solid State **29**, 991 (1987)].
[38] M. S. Brodin, A. O. Gushcha, V. N. Karataev, V. V. Tishchenko, B. E. Derkach, and A. I. Savchuk, Fiz. Tverd. Tela (Leningrad) **30**, 3481 (1988) [Sov. Phys. Solid State **30**, 1999 (1988)].
[39] R. Baltrameyunas, E. Gerazimas, B. E. Derkach, É. Kuokshtis, and A. I. Savchuk, Fiz. Tverd. Tela (Leningrad) **31**, 285 (1989) [Sov. Phys. Solid State **31** (9), 1640 (1989)].
[40] A. I. Savchuk, B. E. Derkach, P. P. Vatamanyuk, A. V. Savitskiĭ, and K. S. Ul'yanitskii, Fiz. Tekh. Poluprovodn. **22**, 512 (1988) [Sov. Phys. Semicond. **22**, 312 (1988)].
[41] A. I. Savchuk and B. E. Derkach, Fiz. Tverd. Tela (Leningrad) **30**, 3171 (1988) [Sov. Phys. Solid State **30**, 1826 (1988)].
[42] H. Kett, W. Gebhardt, U. Krey, and J. K. Furdyna, J. Magn. Magn. Mater. **25**, 215 (1981).
[43] E. Kierzek-Pecold, W. Szymanska, and R. R. Galazka, in *Proc. XII Conf. on Physics of Semiconductor Compounds* (R. R. Galazka and J. Rouluszkiewicz, eds.), Jaszowiec, Poland, 1983, p. 368.
[44] E. Kierzek-Pecold, W. Szymanska, and R. R. Galazka, Solid State Commun. **50**, 685 (1984).
[45] A. Mycielski, J. Wrobel, and M. Arciszewska, in *Proc. XII Conf. on Physics of Semicond. Compounds* (R. R. Galazka and J. Rouluszkiewicz, eds.), Jaszowiec, Poland, 1983, p. 404.
[46] A. Mycielski, C. Rigaux, M. Menant, T. Dietl, and M. Otto, Solid State Commun. **50**, 257 (1984).

[47] C. Rigaux, A. Mycielski, G. Barilero, and M. Menant, Phys. Rev. B **34**, 3313 (1986).
[48] Y. Zhou, C. Rigaux, A. Mycielski, and M. Menant, in *Proc. XIX Intern. Conf. on Physics of Semiconducors* (W. Zawadzki, ed.), Inst. Phys. Pol. Acad. Sci., Warsaw, 1988, Vol. 2, 1551.
[49] D. Scalbert, J. Cernogora, and C. Benoit a'la Guillaume, in *Proc. XIX Intern. Conf. on Physics of Semiconductors* (W. Zawadzki, ed.), Inst. Phys. Pol. Acad. Sci., Warsaw, 1988, Vol. 2, 1547.
[50] C. Rigaux, A. Mycielski, G. Barilero, and M. Menant, *Proc. XVIII Intern. Conf. on Physics of Semiconductors*, Stockholm, 1986, p. 220.
[51] L. Lundgren, P. Svedlindh, and O. Beckman, J. Magn. Magn. Mater. **25**, 33 (1981).
[52] S. Geschwind, A. T. Ogielski, G. Devlin, J. Hegarty, and P. Bridenbaugh, J. Appl. Phys. **63**, 3291 (1988).
[53] R. R. Galazka, S. Nagata, and P. H. Kessom, Phys. Rev. B **22**, 3344 (1980).
[54] M. Ayadi, P. Nordblad, J. Ferre, A. Mauger, and R. Triboulet, J. Magn. Magn. Mater. **54**, 1223 (1986).
[55] Z. Koziol and A. Golnik, Acta Phys. Polon. A **71**, 159 (1987).
[56] W. Walecki and A. Twardowski, Acta Phys. Polon. A **75**, 313 (1989).
[57] E. Kierzek-Pecold, W. Szymanska, and J. Ginter, J. Magn. Magn. Mater. **50**, 243 (1985).
[58] E. Kierzek-Pecold, W. Szymanska, and J. Ginter, Acta Phys. Polon. A **69**, 1063 (1986).
[59] S. Y. Yuen, P. A. Wolff, P. Becla, and D. Nelson, J. Vac. Sci. Technol. A **5**, 3040 (1987).
[60] R. Romestain, S. Geschwind, and G. E. Devlin, Phys. Rev. Lett. **35**, 803 (1986).
[61] J. P. Van der Ziel, P. S. Pershan, and L. D. Malstrom, Phys. Rev. Lett. **15**, 190 (1965).
[62] V. S. Zapasskiĭ and P. P. Feofilov, Usp. Fiz. Nauk **116**, 41 (1975) [Sov. Phys. Usp. **18**, 323 (1975)].
[63] S. M. Ryabehcnko, Yu. G. Semenov, and O. V. Terletskiĭ, Zh. Eksp. Teor. Fiz. **82**, 951 (1982) [Sov. Phys. JETP **55**, 557 (1982)].
[64] D. D. Awschalom, J. Warnock, and S. Molnar, Phys. Rev. Lett. **58**, 812 (1987).
[65] H. Krenn, W. Zawadzki, and G. Bauer, Phys. Rev. Lett. **55**, 1510 (1985).
[66] B. L. Gel'mont, V. I. Ivanov-Omskiĭ, and Ė. I. Tsidil'kovskiĭ, *Abstracts of Reports at XI All-Union Conf. on Semiconductor Physics* (in Russian), Kishinev, 1988, Vol. 1, p. 78.
[67] T. Koyanagi, K. Matsubara, H. Takaoka, and T. Takagi, J. Appl. Phys. **61**, 3020 (1987).
[68] T. Koyanagi, K. Nakamura, K. Yamano, and K. Matsubara, J. Magn. Soc. Japan **12**, 187 (1988).
[69] M. Ortenberg, Lect. Notes Phys. **177**, 451 (1983).
[70] T. Watanabe, K. Yamano, T. Koyanagi, and K. Matsubara, J. Magn. Soc. Japan **11**, 317 (1987).
[71] M. J. Weber, Faraday Rotator Materials, Lawrence Livermore Laboratory, Univ. of California, 1981.
[72] M. J. Weber, Proc. Soc. Photo-Opt. Eng. (Larry G. Deshazer, ed.) **681**, 75 (1987).
[73] A. M. Glass, Science **235**, 1003 (1987).
[74] A. E. Turner, R. L. Gunshor, and S. Datta, Appl. Opt. **22**, 3152 (1983).
[75] G. Fischer, J. Opt. Commun. **8**, 18 (1987).
[76] M. A. Butler, S. J. Martin, and R. J. Baughman, Appl. Phys. Lett. **49**, 1053 (1986).
[77] M. A. Butler and S. J. Martin, in *Proc. Transducers '85*, Philadelphia, 1985, p. 316.
[78] M. A. Butler, Solid State Commun. **62**, 45 (1987).
[79] D. A. Aksionov (Aksenov), V. I. Konov, P. I. Nikitin, A. M. Prokhorov, A. I. Savchuk, A. V. Savitskiĭ, and K. S. Ulyanitskiĭ, *Abstracts of Reports V Intern. Conf. on Solid-State Sensors and Actuators*, Montreux, Switzerland, 1989, p. 252.
[80] D. A. Aksionov (Aksenov), V. I. Konov, P. I. Nikitin, A. M. Prokhorov, A. I. Savchuk, A. V. Savitskii, and K. S. Ulyanitskii, Sensors Actuators, No. 23, 875 (1990).
[81] N. F. Andreev, V. G. Gass, S. V. Zhakov, T. V. Zarubina, S. V. Kuznetsov, M. A. Novikov, O. V. Palashov, G. A. Pasmanik, P. S. Razenshtein, V. S. Rastegaev, A. I. Savchuk, and L. A. Smirnova, Preprint IPF AN SSSR No. 251, Gor'kii, USSR, 1989, p. 22.
[82] S. N. Barybin, A. N. Grigorenko, V. I. Konov, and P. I. Nikitin, Abstracts of Reports IV European Conf. EPROSENSORS, Karlsruhe, Germany, 1990 (to be published in Sensors Actuators, 1991).

Translated by A. Zaslavsky